2019 IMEKO TC-4 International Conference on
Metrology for Archaeology and Cultural Heritage
Florence, Italy, December 4-6, 2019

Recent developments on portable XRF scanner

Lins, S.A.B.[1,2], Gigante, G.E.[1], Cesareo, R.[3], Ridolfi, S.[4]

[1] *La Sapienza Università di Roma, Via Antonio Scarpa 14/16 – 00161, Rome, Italy,*
sergio.lins@roma3.infn.it, giovanni.gigante@uniroma1.it
[2] *Surface Analysis Laboratory INFN Roma Tre, Via della Vasca Navale 84 – 00146, Rome, Italy*
sergio.lins@roma3.infn.it
[3] *Università degli Studi di Sassari, Istituto di Matematica e Fisica, Via Vienna 2 – 07100, Sassari, Italy*
cesareo@uniss.it
[4] *Ars Mensurae, Via Vincenzo Comparini 101 – 00188, Rome, Italy,*
stefano@arsmensurae.it

***Abstract* – A prototype X-ray fluorescence (XRF) scanner was developed with the aim of being reliable and portable, best suiting the needs of cultural heritage scientists who constantly face the difficulty of *in-situ* analysis. The instrument constructed is composed of an exchangeable scanning head (X-ray tube and detector), a motorized x-y stage with a controlling interface and a laptop. With the small stage, it can scan areas up to 20 x 20 cm^2 with a lateral resolution of 1 mm. The system can be transported inside a standard airplane cabin trolley and weights no more than 10 Kg. The controlling interface was programmed in LabView© and the data evaluation is performed on-the-go with a *custom-made* algorithm. The system has been put to test with a variety of materials and some results are discussed.**

I. INTRODUCTION

X-ray fluorescence (XRF) is a firmly stablished technique, which possesses several fundamental pre-requisites for cultural heritage scientists: it can be performed *in-situ*, it's fast, efficient, safe, non-destructive and can be used to investigate a variety of materials, from glazed ceramics, to paintings and metals [1] [2] [3] [4] [5]; yielding information such as pictorial technique, conservation state, authenticity and manufacturing. Nonetheless, when dealing with inhomogeneous and stratified samples – which is often the case of cultural heritage objects – the results obtained can lead to misleading interpretations [6] [7].

An extrapolation of traditional XRF spot-analysis to an extra dimension, providing a bi-dimensional matrix of spectra and covering a large superficial area is commonly labelled as macro XRF scanning (MA-XRF) [8]. This approach can provide the simultaneous mapping of chemical elements, underlining their spatial distribution and revealing hidden information [9]. Since 2008, when elemental distribution maps from a medium sized Van Gogh painting have come to light, revealing a hidden portrait [10], MA-XRF has been further optimized and incorporated into mobile instruments to perform *in-situ* analysis [8] [9] [11] [12]. The development of mobile scanners has become a trend, and different models have been created, either by companies or universities.

Being able to transport instruments and perform *in-situ* analysis is of utmost interest for cultural heritage scientists, seen that it's very unlikely that a priceless artwork will leave the tutelage of the museum save rare exceptions.

MA-XRF investigations are performed by using an X-ray tube and one (or more) detector(s), acquiring one spectrum for each pixel throughout the sample surface. There are few different *formats* when it comes to the scanning geometry itself – besides the classical tube-sample-detector geometry. First, whether the scanning head or the sample will move with the x-y motorized stage and second whether they will be positioned vertically or horizontally [13] [14]. Another critical point in the scanning systems is the beam focusing and detection efficiency. Two common choices for focusing the beam are pinhole collimators and polycapillary lenses, the former being a considerably cheaper option, but with the drawback of reducing the beam intensity and thus increasing the dwell-time (time spent on each pixel) [15].

In order to acquire a large image within a satisfactory time window and a relatively "good" resolution, a fine balance must be found between the spot size, focusing optics and detection efficiency. Commercial MA-XRF scanners that overcome these problems are currently available, some being mobile (but not portable) while others being tabletop instruments [14]. Yet, the commercial options are often either expensive or bulky.

As an alternative, a low-cost and portable MA-XRF scanner was developed by *Ars Mensurae* and the *Istituto Nazionale di Fisica Nucleare* (INFN) Roma TRE Division. The prototype is composed of an exchangeable scanning head, a motorized x-y stage with a controlling unit and a laptop. The scanning head can be easily changed between different x-y stages to suit different needs. Within

the current framework, two stages are operational. One, portable, for scanning areas up to 20 x 20 cm^2 and a larger, mobile one, for scanning areas up to 100 x 100 cm^2. The controlling interface (CI) was programmed in LabView and features an "almost live" display of the counts map and the last acquired spectrum. The same CI controls both small and large motorized stages, thus requiring a minimal effort to change from a portable to a mobile scanner following a *plug-and-play* approach.

The developed system has been put to test with different materials of cultural science interest: gilt and painted leathers, painted copper plates, corroded alloys, sediment blocks and canvas paintings. Some of these results have been already published elsewhere [16]. The current contribution highlights the system specifications and potentials as well as some preliminary results.

II. EXPERIMENTAL

A. The Scanner

The scanner itself can be subdivided into three main parts: scanning head, motorized stage and controlling unit (Fig. 1). The scanning head is composed of a low-power Ta-target Moxtek® X-ray tube attached to an exchangeable collimator (2 mm diameter, 21 mm in length) – *or* a low-power Au-target AMPTEK X-ray tube – and a silicon drift (SDD) detector. The detector is a lightweight and low-power (180 g and 2.5 W) X-123SDD from AMPTEK® with a 125 eV resolution at Mn Kα-Line.

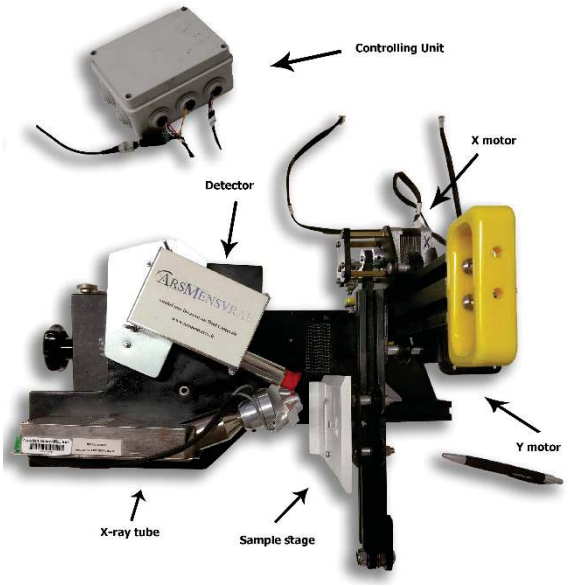

Fig. 1. Portable scanning system

The focus between the scanning head and sample is set manually with the aid of a laser triangulation system. Spot size is dictated by the X-ray focusing optics chosen (collimator). At about 1 cm from the sample's surface it is of roughly 2 mm diameter for both tubes.

The motorized stage can also be chosen according to the application and necessity. Here we highlight the use of the smaller stage, adapted from a low-cost 3D printer and capable of scanning areas up to 20 x 20 cm^2 with a step resolution up to 100 microns. The stage is lightweight and portable, fitting comfortably inside a cabin trolley. Last, the controlling unit (CU) is composed of a custom-made printed board coupled to a National Instruments® board and linked to a laptop by a standard universal serial cable (USB).

The *format* adopted in both portable and mobile setups is vertical. In the portable setup, due to mechanical and dimensional constraints, the sample is moved by the x-y stage instead of the scanning head. The movement is controlled by the CU and follows a "serpent" pattern. The spectra acquisition is made step-by-step. The CI sends the signal to start the spectrum acquisition and only when its finished with the current pixel, the stage will move to the next one and so on.

Due to the inherent low-power nature of the system, it is possible to run small area analysis solely on batteries, transforming it into a truly portable system.

B. Controlling Interface and Data analysis

The CI was programmed on LabView. It controls the motors movement, spectrum acquisition/writing and displays a near-live time *count-map* of the area under analysis. The count-map (or density map) is a 2D image where each pixel is represented by the total counts of the associated pixel-spectrum. This image is refreshed and normalized after each spectrum is acquired through simple array operations, thus consuming little resources so the user can ascertain the analysis status and quality by viewing the last acquired spectrum and the count-map on screen.

The evaluation of the data itself, *i.e.* plotting derived spectra and the individual or combined elemental distribution maps is performed only after the acquisition is finished. Since the quality of the data can be checked during the analysis, the fact that the data can only be processed and evaluated after the often hour-long acquisition process is of little concern.

The *custom-made* analysis algorithm can generate elemental maps by different imaging methods, easily chosen and changed by the user. To improve processing time, all mca files are packed into one cube file. When packing the cube file, the spectra backgrounds are also computed and packed together to save on processing time afterwards. The background stripping method implemented so far is the SNIPBG method and its described in detail elsewhere [17].

For the imaging methods, the traditional region of interest (ROI) imaging technique (here referred to as *simple ROI*) has been implemented and adapted. Simple

ROI automatically selects the ROI as a span of 2*FWHM ± 10% centered at the theoretical peak energy by verifying the summation derived spectrum (for each peak of interest), meaning that all it takes for the image to be generated is the name of the chemical element of interest.

An *auto ROI* method was also developed, where the algorithm searches each spectrum for the presence of the element of interest, by following some pre-defined criteria: signal to noise ratio (SNR), second differential check and distance from the theoretical peak center. In this method, each spectrum is smoothed by a Savitzky-Golay filter [18] to render easier the detection of the peak. The net-area is calculated over the raw, non-smoothened spectrum. This method has the advantage of detecting rare occurrences (such as those only visible by the maximum pixel spectrum [19]) at the cost of an increase in processing time. A comparison between *simple* and *auto* imaging methods is show in Fig. 2.

A third method is also available, fitting the spectra one by one through the least-squares fitting method from PyMca [20] and incorporated into the algorithm. The fitting configuration is universal, *i.e.* one single configuration and set of elements is considered for every single spectrum. If the sample is extremely inhomogeneous, this can lead to few under or over estimations. Nonetheless, after each image is created, the area evaluated is recorded and can be confronted with the summation spectrum and background estimation for a visual check, so if any under of over estimation is to happen, the user can view them and select another imaging technique found more suitable for that sample.

Some extra functionalities were also implemented to help with data interpretation. The summation spectrum can be confronted with all the emission lines of a given element including the spread of the lines following a gaussian distribution. A built-in image analysis system is also embedded, to render better the visualization of images by combining threshold or low-pass filters with an iterative smoothening filter. The user can visualize up to two images at the same time and easily correlate them.

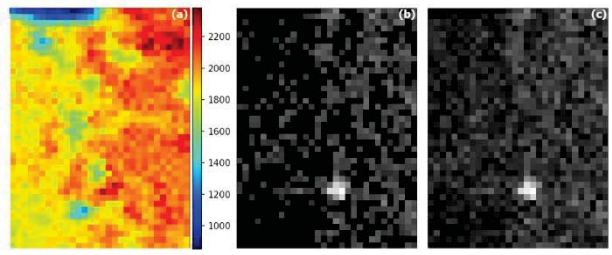

Fig. 2. Count-map (a), auto (b) and simple (c) ROI maps for Mn-Kα. Auto ROI image is filtered.

III. RESULTS

The portable scanner prototype has been tested with a variety of materials of cultural heritage interest. A systematic analysis was carried over painted and gilt leather pieces from the XVII century to shed light on the pigments and pictorial technique and are available in more detail elsewhere [16]. The elemental distribution maps could clearly pin-point the copper-based pigment, blue pigment (identified as indigo mixed with lead-white) and attest the presence of lead-white as a preparatory layer, as well as suggest the use of potash alum and lime or soda ash during the tanning and un-hairing process, respectively.

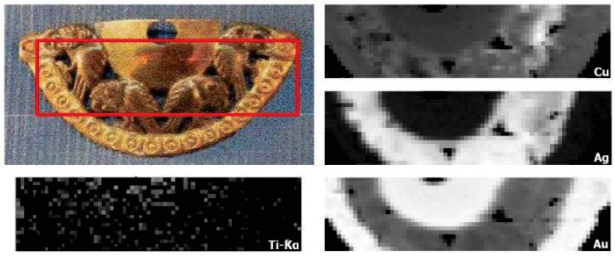

Fig.3. Copper, silver, gold and titanium distribution on a Peruvian nose ornament.

A Peruvian nose ornament was also analyzed. The analyzed area was of 1.8 x 7.0 cm^2 with a dwell-time of 10 seconds and totalizing 1260 pixels. The elemental maps clearly demonstrated the use of interspersed gold-silver-copper alloys (tumbagas). A curious inhomogeneity in the alloy was detected, presenting a significant higher quantity of copper than in the rest of the object (Fig. 3 above). Copper, gold and silver maps represents the sum of alpha and beta lines (K-lines for copper and silver and L-lines for gold) and were obtained with the *auto ROI* imaging method. A threshold filter was applied over the titanium map to enhance its visualization.

Maximum pixel spectrum (MPS) showed the presence of titanium, otherwise overlooked by traditional methods (Fig. 4). Nonetheless, the reasons for which titanium is present in this particular sample are still unclear.

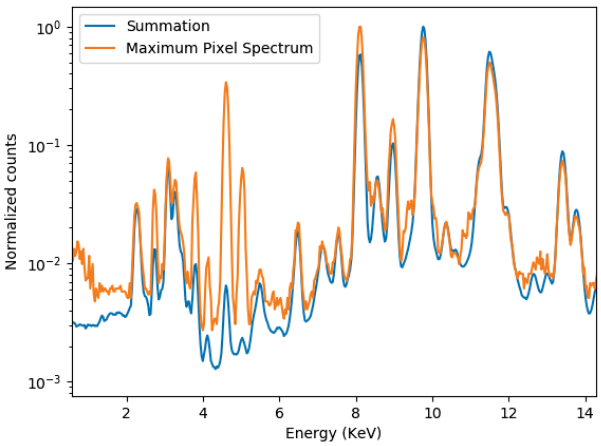

Fig.4. Normalized summation and MPS spectra. Discrepancy in Ti signal around 4.5 KeV.

The largest sample analyzed so far with the portable prototype was of 5.6 x 6.5 cm^2 with a dwell-time of 2

seconds and a total acquisition time of about 2h. The mobile version, instead, was put to test with a slightly larger sample (which would still fit under the portable model) of 9.7 and 7.7 cm^2 with a dwell-time of 1 second.

IV. CONCLUSIONS

The scanner has performed greatly considering its low-power nature, portability and incredible lightweight. The possibility to easily change between a portable and mobile version according to the application has proven to be a very positive and useful feature, maintaining the cost of the instrument as low as possible. Still there are places for improvements and tweaks within the current framework. The prototype still lacks some functionalities, as a z-axis movement for automatic focusing paired with the laser triangulation system.

The data analysis software and its *custom-made* tools have proven to be very versatile and helpful in interpreting low-signal and noisy data. Automatic peak selection, net-area estimation and background stripping allowed the analysis to be as simple and straightforward as possible.

FUNDING

This project has received funding from European Union's Horizon 2020 research and innovation program under Marie Skłodowska-Curie Actions Innovative Training Networks grant agreement N. 766311.

REFERENCES

[1] Z.Duan, J.Liu, Q.Jiang, Q.Pan, L.Cheng, *"A type of portable micro-EDXRF spectrometer with laser displacement sensor"* Nuclear Instruments and Methods in Physics Research, Section B: Beam Interactions with Materials and Atoms, vol.442, 2019, pp.13-18.

[2] R.Cesareo, A.Bustamante, R.F.Jordan, A.Fernandez, S.Azeredo, R.T.Lopes, W.Alva, L.Chero, A.Brunetti, G.E.Gigante, S.Ridolfi, *"Gold and silver joining technologies in the moche tombs Señor de Sipán and Señora de Cao jewellery"* Acta IMEKO, vol.7, No.3, 2018, pp.3-7.

[3] A.Brunetti, A.Depalmas, F.Di Gennaro, A.Serges , N.Schiavon, *"X-ray fluorescence spectroscopy and Monte Carlo characterization of a unique nuragic artifact (Sardinia, Italy)"*, Spectrochimica Acta - Part B Atomic Spectroscopy, vol.121, 2016, pp.18-21.

[4] S.Ridolfi, M.Laurenzi Tabasso, A.Askari Chaverdi, P.Callieri, *"The Finishing Technique of the Stone Monuments of Persepolis: Further Studies and New Findings Through the Use of Non-Destructive Analytical Techniques"*, Archaeometry, vol.281, 2019, pp.271-281.

[5] S.Ridolfi, *"Gilded copper studied by non-destructive energy-dispersive X-ray fluorescence"*, Insight: Non-Destructive Testing and Condition Monitoring, vol.60, No.1, 2018, pp.37-41.

[6] R.Cesareo, A.Bustamante, J.Fabian, C.Calza, M.Dos Anjos, R.T.Lopes, C.Elera, I.Shimada, V.Curay, *"Energy-dispersive X-ray fluorescence analysis of a pre-Columbian funerary gold mask from the Museum of Sicán, Peru"*, X-Ray Spectrometry, vol.39, No.2, 2010, pp.122-126.

[7] A.Brunetti, J.Fabian, C.W.La Torre, N.Schiavon, *"A combined XRF/Monte Carlo simulation study of multilayered Peruvian metal artifacts from the tomb of the Priestess of Chornancap"*, Applied Physics A: Materials Science and Processing, vol.122, No.6, 2016, pp.1-8.

[8] E.Ravaud, L.Pichon, L.Laval, V.Gonzalez, M.Eveno, T.Calligaro, *"Development of a versatile XRF scanner for the elemental imaging of paintworks"*, Applied Physics A, vol.122, No.1, 2016, pp.1-7.

[9] P.Romano, C.Caliri, S.Di Martino, L.Pappalardo, F.Rizzo, H.Santos, *"Real-time elemental imaging of large dimension paintings with a novel mobile macro X-ray fluorescence (MA-XRF) scanning technique"*, Journal of Analytical Atomic Spectrometry, vol.32, No.4, 2017, pp.773-781.

[10] J.Dik, K.Janssens, G.Van der Snickt, L.Van der Loeff, K.Rickers, M.Cotte, *"Visualization of a Lost Painting by Vincent van Gogh Using Synchrotron Radiation Based X-ray Fluorescence Elemental Mapping"*, Anal. Chem., vol.80, No.16, 2008, pp.6436-6442.

[11] D.Howard, M.De Jonge, D.Lau, D.Hay, M.Varcoe-Cocks, C.Ryan, R.Kirkham, G.Moorhead, D.Paterson, D.Thurrowgood, *"High-definition X-ray fluorescence elemental mapping of paintings"*, Analytical Chemistry, vol.84, No. 7, 2012, pp.3278-3286.

[12] R.Cesareo, S.Ridolfi, A.Brunetti, R.T.Lopes, G.E.Gigante, *"First results on the use of a EDXRF scanner for 3D imaging of paintings"*, Acta IMEKO, vol.7, No. 3, 2018, pp.8-12.

[13] T.Trojek, D.Trojková, "Several approaches to the investigation of paintings with the use of portable X-ray fluorescence analysis", Radiation Physics and Chemistry, vol.116, 2015, pp.321-325.

[14] M.Alfeld, J.V.Pedroso, M.Van Eikema Hommes, G.Van Der Snickt, G.Tauber, J.Blaas, M.Haschke, K.Erler, J.Dik, *"A mobile instrument for in situ scanning macro-XRF investigation of historical paintings"*, Journal of Analytical Atomic Spectrometry, vol.28, No.5, 2013, pp.760-767.

[15] C.Polese, S.B.Dabagov, A.Esposito, A.Liedl,

D.Hampai, C.Bartùl, M.Ferretti, *"Proposal for a prototype of portable μxRF spectrometer"*, Nuclear Instruments and Methods in Physics Research, Section B: Beam Interactions with Materials and Atoms, vol.355, 2015, pp.281-284.

[16] I.Morena, V.Graziani, S.Lins, S.Ridolfi, P.Branchini, A.Fabbri, G.Ingo, G.Di Carlo, L.Tortora, *"Exploring Manufacturing Process and Degradation Products of Gilt and Painted Leather"*, Applied Sciences, vol.9, No.15, 2019.

[17] P.Van Espen, *"Chapter 4: Spectrum Evaluation"*, in Handbook of X-ray spectrometry, Marcel Dekker, Inc., 2002, pp.239-339.

[18] P.A.Gorry, *"General Least-Squares Smoothing and Differentiation by the Convolution (Savitzky-Golay) Method"*, Analytical Chemistry, vol.62, 1990, pp.570-573.

[19] D.S.Bright, D.E. Newbury, *"Maximum pixel spectrum: A new tool for detecting and recovering rare, unanticipated features from spectrum image data cubes"*, Journal of Microscopy, vol.216, No.2, 2004, pp.186-193.

[20] V.A.Solé, E.Papillon, M.Cotte, P.Walter, J.Susini, *"A multiplatform code for the analysis of energy-dispersive X-ray fluorescence spectra"*, Spectrochimica Acta - Part B Atomic Spectroscopy, vol.62, No.1, 2007, pp.63-68.

[21] R.Cesareo, *"Non-destructive EDXRF-analysis of the golden haloes of Giotto's frescos in the Chapel of the Scrovegni in Padua"*, Nuclear Instruments and Methods in Physics Research, Section B: Beam Interactions with Materials and Atoms, 2003, pp.133-137.